Coupling of Raman Radial Breathing Modes in Double-Wall Carbon Nanotubes and Bundles of Nanotubes

Si-ping Han and William A. Goddard III*

Materials and Properties Simulation Center, California Institute of Technology, Pasadena, California 91125

Received: July 2, 2008; Revised Manuscript Received: February 19, 2009

Measurements of the radial breathing modes from Raman Spectroscopy have been most useful in characterizing the diameters of single-wall carbon nanotubes (SWNT), where there is a simple monotonic relationship between frequency and diameter. Similar correlations have also been used to predict sizes for double and multiple wall nanotubes and for bundles of SWNT. However this can lead to significant errors because the relationship between frequencies and diameter is much more complicated for DWNT. This is because of couplings between the vibrations of various walls. To provide guidance in such assignments we used the GraFF atomistic force field to predict the in-phase and counter-phase radial breathing modes (RBMs) of double wall carbon nanotubes (DWNTs) over a broad range of inner and outer diameters and chiralities. We then developed an analytical model to describe the RBMs of dispersed DWNTs. This enables the inner and outer shell diameters to be extracted from pairs of RBM peaks. We find that nanotubes bundles show significant dependent peak broadening and shifting compared to dispersed nanotubes. For bundles of SWNT and DWNT, the relationships are much more complicated.

High-quality double-wall carbon nanotubes (DWNT) can now be produced in quantity using catalytic chemical vapor deposition,[1] arc discharge,[2] and a variety of other methods.[3] The unique two-layer structure of DWNTs confers advantages such as defect-free inner shells[9] and better field emission properties than single-wall and multiwall carbon nanotubes.[4] Recent density functional theory calculations suggest that, for small diameter DWNTs with closely spaced shells, intershell electronic structure coupling could lead a pair of semiconducting shells to act collectively as a single metallic wire. Thus, it may be possible to produce uniformly metallic DWNTs by constraining diameter.[5]

Further development of DWNTs' technological potential would benefit from better characterization of their inner and outer chiralities and diameters. A commonly used and relatively simple method for diameter characterization is assignment based on the radial breathing mode (RBM) peaks in the Raman spectra. However, for DWNT, calculations show that when the intershell separation approaches the graphite interlayer distance (∼3.4 Å[10]) the inner and outer walls interact to split the RBMs. Thus, the common assumption that each shell in a DWNT vibrates independently with the RBM appearing at the same places as for the corresponding single-wall carbon nanotube (SWNT) produces systematic errors.

To predict the RBM for DWNTs, we used atomistic force field simulations to map the in-phase and counter-phase RBMs of dispersed individual commensurate and incommensurate DWNTs over a broad range of inner and outer diameters and chiralities. We find that a continuum model treating the DWNT as two concentric uniform elastic shells coupled by a van der Waals force[7] accurately fits our results using four free parameters. This simple formulation allows rapid solutions for both the forward problem of calculating RBMs from given diameters and the inverse problem of getting diameters from pairs of given RBMs. (A simple Python script for doing these calculations is included in the Supporting Information.) Since many DWNT samples are probed in a form where the nanotubes are bundled, we also simulated homogeneous DWNT bundles, which showed diameter-dependent broadening and shift of RBM peaks from those of individual nanotubes due to internanotube dispersive coupling. Collectively, our results should enable more accurate interpretation of RBM data for DWNTs.

In this paper, we will refer to the chirality of the inner wall as (n_i, m_i) and that of the outer wall as (n_o, m_o). We define the inner (d_i) and outer (d_o) diameters to be the diameters of the imaginary cylindrical shells drawn through the centers of the carbon atoms in the inner and outer walls. The separation between the inner and outer shells is $\Delta = (d_o - d_i)/2$. To a good approximation, the diameter of each shell, d, is determined by its chirality: $d = c\sqrt{n^2 + m^2 + nm}$, where c is the C−C equilibrium bond distance in graphene. For $\Delta < 3.0$ Å, our simulations show that repulsion between the inner and outer shells distorts C−C bond distances, leading d_i and d_o to deviate slightly from the simple relation given above.

All carbon nanotubes were simulated in vacuum using the GraFF atomistic force field fitted to the geometric and elastic properties of graphite crystals.[6] This force field includes a Morse-type description for bond stretches, a cosine-type potential for the angles between adjacent bonds, and a 2-fold torsion term. It uses a Lennard−Jones 12−6 description for the van der Waals interaction.[6] This force field leads to an accurate prediction of the structures and vibrational properties of C_{60} and C_{70} molecules and of the cohesive energy of fullerene crystal.[6] It is expected to give accurate geometries, energies, elastic constants, and intershell rotational and translational barriers for both large and small diameter DWNTs.

Optimal geometries for carbon nanotubes were obtained by energy and force minimization, resulting in C−C bond distances of approximately 1.43 Å. The enthalpy of formation of a (10,10) SWNT was 2.50 kcal/(mole atoms) compared to a graphene sheet from graphite. The vibrational normal modes of nanotubes

* To whom correspondence should be addressed. E-mail: wag@wag.caltech.edu.

10.1021/jp805828g CCC: $40.75
Published on Web 04/23/2009

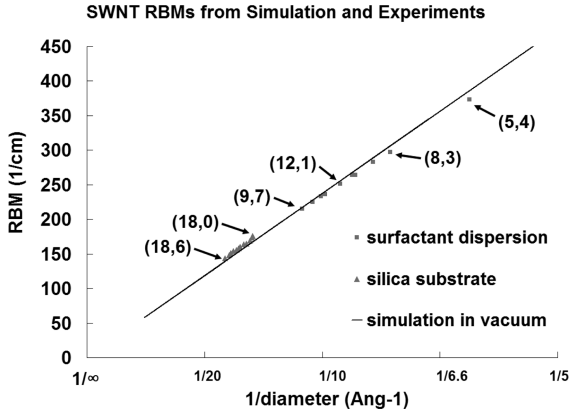

Figure 1. Experimentally observed RBM frequencies for SWNTs of various chiralities and diameters. The diameters are calculated from the reported chiralities using $d = a(m^2 + n^2 + mn)^{1/2}$. The black line shows that eq 1 with $a = 237.5$ cm^{-1} and $b = 0.0$ cm^{-1} leads to good agreement with experiment.

were calculated from optimized geometries by diagonalization of the Hessian. The (10,10) SWNT's radial breathing mode in vacuum was 173.15 cm^{-1}.

As a test, we calculated the RBMs of individual SWNTs. These modes obey the following equation

$$f = \frac{a}{\text{diameter}} + b \qquad (1)$$

Fitting of a and b using 34 armchair, zigzag, and chiral SWNTs leads to $a = 237.5$ cm^{-1} and $b = 0.0$ cm^{-1}. Figure 1 compares eq 1 using these values for a and b to experimental results for individual SWNTs dispersed on SiO_2 substrate ($a = 248$ cm^{-1}and $b = 0.0$ cm^{-1})[12] and those dispersed in fluid with sodium dodecyl sulfate surfactant ($a = 223.5$ cm^{-1} and $b = 13.5$ cm^{-1}).[11] Thus, our calculations lead to good agreement with experiment.

Commensurate zigzag DWNTs with (n_i,0) inner and (n_o,0) outer shells were constructed with $n_i = 10$, 15, 20 and $n_o = n_i + 5$ to $n_i + 13$. This allowed fine-grained sampling of the range of diameters and separations obtained from selective synthesis methods while minimizing the number of atoms in the unit cell. Each nanotube was periodic in the axial direction and effectively isolated in the transverse directions. Optimal geometries were again obtained by force and energy minimization. A comparison of inner and outer shell diameters to corresponding SWNT diameters showed that the change in diameter due to intershell coupling was less than 1% for $\Delta > 3.1$ Å and approximately 2% for 3.0 Å $\leq \Delta \leq 3.1$ Å. DWNTs with $d_i \leq 10$ Å were more distorted than those with larger inner diameters. For incommensurate DWNTs, unit cells were lengthened until the length mismatch between the inner and outer shells was less than 1%.

In-phase and counter-phase RBMs for our DWNT models are plotted in Figure 2. They show that, for $\Delta < 3.7$ Å, there is significant deviation of both types of RBMs from the RBMs of corresponding SWNTs. For example, the (15,0)@(23,0) nanotube with $\Delta = 3.22$ Å had an in-phase RBM of 146.03 cm^{-1} and a counter-phase mode of 235.11 cm^{-1}. On the other hand, the (23,0) SWNT's RBM was 130.51 cm^{-1}and the (15,0) SWNT's RBM was 199.31 cm^{-1}.

Our simulations show that the distortion of bond lengths in the outer shell is minimal (Table 1, Supporting Information) and does not account for the calculated change in the RBM frequencies. Instead, it is the van der Waals coupling that causes

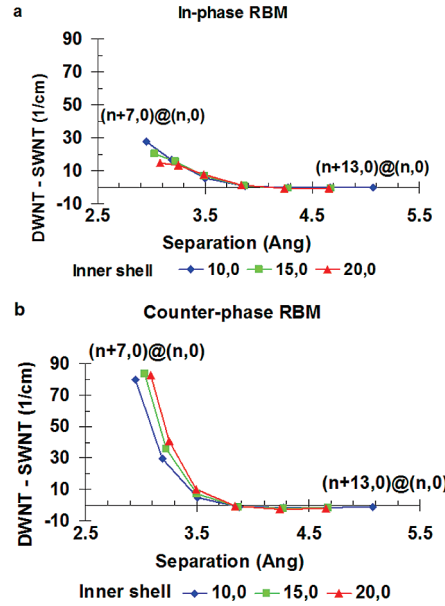

Figure 2. (a) Difference when the RBM of the outer shell's corresponding SWNT is subtracted from the in-phase RBM of a DWNT. (b) Difference when the inner-shell SWNT RBM is subtracted from the counter-phase DWNT RBM.

TABLE 1: RBM data from Ref 8 Analyzed Using the Continuum Model for Dispersed and Bundled DWNT RBMs[a]

counter-phase (cm^{-1})	on-phase (cm^{-1})	d_i (Å)	d_o (Å)	Δ (Å)
385	150	6.15994	15.7382	4.78913
		13.15222	18.77304	2.81041
	158	6.15792	14.92034	4.38121
		12.3228	17.95668	2.81694
	197	*6.4182*	*12.91342*	*3.24761*
		9.00318	14.75078	2.8738
	227	no solution		
	257	no solution		
257	**150**	*9.4856*	*16.4328*	*3.4736*
		12.28984	*18.4547*	*3.08243*
	158	*10.17638*	*16.66472*	*3.24417*
		10.79442	*17.12882*	*3.1672*
	197	no solution		

[a] The most plausible counter-phase RBM candidate peaks from analysis of raw data are shown in bold font, and plausible dimensions of inner and outer nanotubes are italic font. Nanotubes with intershell separation smaller than 3.0 Å are energetically unfavorable.

the RBM shift. A question then arises. For nanotubes with similar inner and outer diameters, does RBM depend on the chiralities of each shell? Since experimental studies have shown that the friction between concentric shells of multiwall carbon nanotubes is small[13] and there is no correlation between the chiralities of the inner and outer shells in a DWNT,[15] we assumed that the chiralities were unimportant and constructed the continuum model for the DWNT as two concentric smooth cylindrical elastic shells with homogeneous mass density and van der Waals interaction density. Using this model, we derived functions for calculating the RBMs using d_i and d_o as input. A subsequent review of the literature showed that Wu, Zhou, and Dong reported a similar model.[7] Here, we briefly explain our derivation.

We can write the following eigenvalue equations for the normal modes of the coupled shells in mass-weighed coordinates

$$\begin{pmatrix} \frac{k_{ii}}{m_i} & \frac{k_{io}}{\sqrt{m_i}\sqrt{m_o}} \\ \frac{k_{oi}}{\sqrt{m_o}\sqrt{m_i}} & \frac{k_{oo}}{m_o} \end{pmatrix} \cdot \begin{pmatrix} \frac{r_i}{\sqrt{m_i}} \\ \frac{r_o}{\sqrt{m_o}} \end{pmatrix} = -\omega^2 \begin{pmatrix} \frac{r_i}{\sqrt{m_i}} \\ \frac{r_o}{\sqrt{m_o}} \end{pmatrix} \quad (2a)$$

where r_i and r_o are the radii and m_i and m_o the masses per unit length of the inner and outer shells. This has solutions

$$\omega_-^2 = \alpha - \beta\omega_+^2 = \alpha + \beta\alpha = \frac{1}{2}\left(\frac{k_{oo}}{m_o} + \frac{k_{ii}}{m_i}\right)$$

$$\beta = \frac{\sqrt{4(k_{io}k_{oi} - k_{ii}k_{oo})m_i m_o + (k_{oo}m_i + k_{ii}m_o)^2}}{2m_i m_o} \quad (2b)$$

where ω_- is the in-phase RBM with lower frequency and ω_+ is the counter-phase RBM with higher frequency.

The potential energy of the nanotube is just the energies of the corresponding SWNTs plus the van der Waals coupling. We can thus separate each elastic constant k_{xy} into components due to the inherent elasticity of the inner and outer shells and components due to van der Waals coupling

$$k_{ii} = m_i\omega_i^2 + \frac{\partial^2 E_{vdW}}{\partial r_i^2} k_{oo} = m_o\omega_0^2 + \frac{\partial^2 E_{vdW}}{\partial r_0^2} k_{oi}$$

$$= k_{io} = \frac{\partial^2 E_{vdW}}{\partial r_o\, \partial r_i}\omega_i = \frac{a}{2r_i} + b\omega_o = \frac{a}{2r_o} + b \quad (2c)$$

where ω_i and ω_o are the RBM frequencies of SWNT corresponding to the inner and outer shells. The parameters a and b were already determined by fitting to our SWNT RBM calculations. The mass per unit length m_i and m_o of the inner and outer shells are

$$m_i = 2\pi R_i \rho m_o = 2\pi R_o \rho \quad (2d)$$

where R_i and R_o are the relaxed radii of the inner and outer shells and ρ is a constant mass density.

Raman transition are given in wavenumbers with units of cm^{-1}. One can trivially convert between frequencies and wavenumbers using the relationship

$$w = \frac{1}{\lambda} = \frac{\omega}{c_o} \quad (2e)$$

where c_o is the speed of light in vacuum.

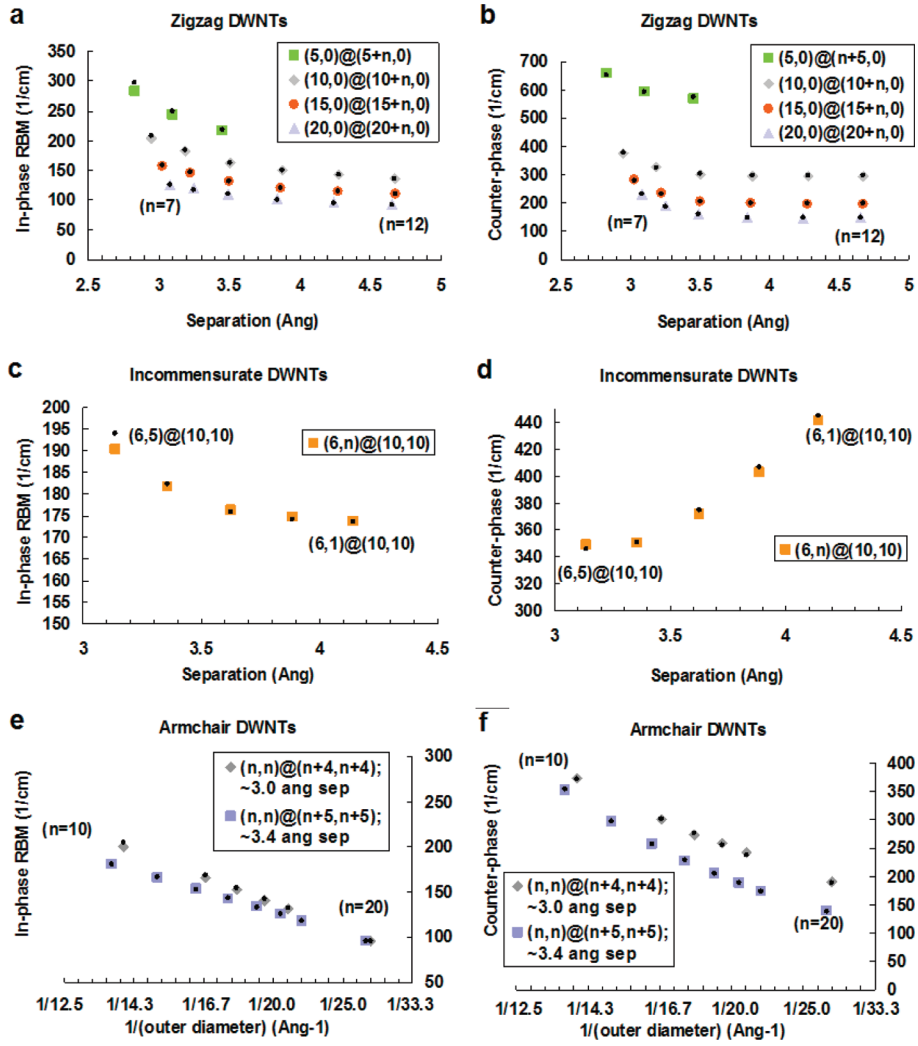

Figure 3. In-phase radial breathing modes are on the left and counter phase modes on the right. The DWNTs in a and b have zigzag inner and outer walls, those in c and d have chiral inner walls and armchair outer walls, and those in e and f have armchair inner and outer walls. (a and b) Inner shell was kept constant and the outer shell changed. (c and d) Outer shell was constant and the inner shell varied. (e and f) Intershell spacing was kept constant while the overall diameter of the DWNTs was varied. All DWNT models were optimized using energy and force minimization. The results show good reproduction of atomistic simulations, shown in color, by the analytical results, shown in black.

The van der Waals interaction energy E_{vdW} is calculated by integrating a Lennard−Jones expression over the two shells in cylindrical coordinates. The radial symmetry of the system gives a simplified expression

$$E_{vdW} = \frac{N_i N_o}{2\pi}\int_0^{2\pi}\int_{-\infty}^{\infty} \mathrm{LJ}\, dl_o\, d\theta_i\, \mathrm{LJ}$$

$$= \varepsilon\left[\left(\frac{\alpha}{R}\right)^{12} - 2\left(\frac{\alpha}{R}\right)^{6}\right]R$$

$$= \left|\sqrt{l_i^2 + r_i^2 + r_o^2 - 2r_i r_o \cos(\theta_i)}\right| \qquad (3a)$$

where N_i and N_o are the numbers of atoms per unit length in the inner and outer shells, α is the distance at which LJ = 0, and α is the van der Waals well depth. Direct integration of LJ yields a closed form expression for E_{vdw}

$$E_{vdW} = \frac{N_i N_o \varepsilon \alpha^6}{640(r_i - r_o)^{10}(r_i + r_o)^9}\left\{-8(r_i - r_o)^2[-40(r_i^2 - r_o^2)^6 + \alpha^6(r_i^2 - r_o^2)(31r_i^4 + 194r_i^2 r_o^2 + 31r_o^4)]K\left(\frac{4r_i r_o}{(r_i + r_o)^2}\right) + [-1280(r_i - r_o)^6(r_i + r_o) + \alpha^6(563r_i^8 + 7604r_i^6 r_o^2 + 16434r_i^4 r_o^4 + 7604r_i^2 r_o^6 + 563r_o^8)]E\left(\frac{4r_i r_o}{(r_i + r_o)^2}\right)\right\} \qquad (3b)$$

where $E((4r_i r_o)/((r_i + r_o)^2))$ is the complete elliptic integral and $K((4r_i r_o)/((r_i + r_o)^2))$ is the complete elliptic integral of the first kind. Substituting the results of eq 3b into eq 2b gives a closed form expression for the two RBMs (see Supporting Information). This expression has four free parameters: a, b, α, and ε. Since a and b are predetermined by fitting to SWNT data, only α and ε are truly free. To find their optimal values, we used Nelder−Mead-type numerical optimization to minimize the squared difference between the calculated RBMs and the simulated RBMs for zigzag DWNTs. This gave α = 3.742 Å, and ε = 0.09090 kcal/mol. For comparison, the LJ parameters for the atomistic graphite force field are α = 3.8050 Å and ε = 0.0692 kcal/mol. Our continuum model parameters differ from the atomistic force field values because the atom centers can be placed in positions to minimize the van der Waals energy.

Figure 3 compares RBMs calculated using the optimized analytical expression with RBMs calculated using atomistic simulations. For all zigzag, armchair, and incommensurate DWNTs in this data set, the difference between the atomistic and analytical counter-phase frequencies is ~1% or less. The errors for most in-phase frequencies are also less than 1% (Table 2, Supporting Information). The exception are the (5,0)@(12,0), (5,0)@(13,0), and (10,0)@(17,0) DWNTs, which lead to errors of over 2%. This is due to greater distortion of the inner and outer shells from their SWNT geometries (Table 1, Supporting Information) and the greater importance of atomic granularity due to smaller numbers of atoms and closer intershell separation. In general, we expect the analytical model to be accurate for DWNTs with intershell separation greater than ~3.0 Å but smaller than ~6 Å. At larger intershell separations, the inner nanotube may move to make better van der Waals contact with a portion of the outer nanotube, thus destroying the concentric cylindrical symmetry assumed for the present model.

An interesting point from Figure 3 is that the analytical expression using α and ε optimized from zigzag DWNT data accurately predicts the RBMs of armchair and incommensurate chiral DWNTs. This demonstrates that the chiralities of the inner and outer shells do not shift RBMs appreciably for DWNTs with the same inner and outer diameters.

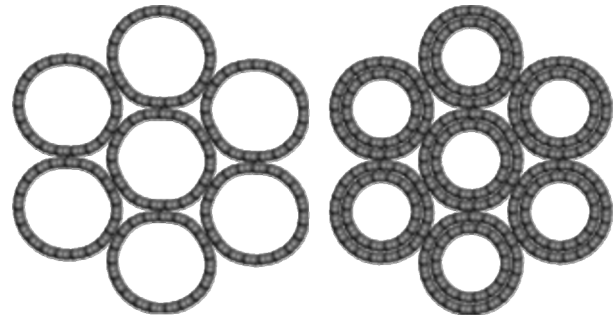

Figure 4. Bundle of seven (20, 20) SWNTs on the left shows distortion as a result of bundling. On the right, seven (20, 20)@(15, 15) nanotubes show similar but much smaller distortion. The diameter for a individual (20, 20) SWNT was 27.3 Å.

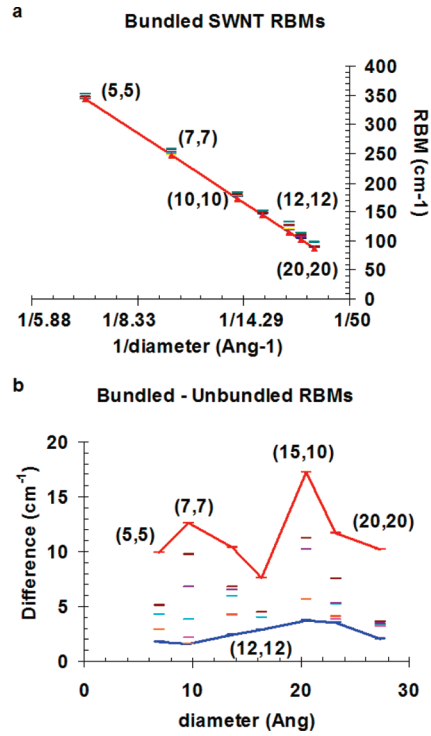

Figure 5. (a) RBM of SWNTs in seven nanotube homogeneous bundles as points, while the RBMs of individual nanotubes are shown as a red line. (b) Difference of the individual SWNT RBM subtracted from the seven modes.

Although our study gives a simple way of calculating RBMs for individual DWNTs, most experimental RBM data reported in the literature are taken on nanotube bundles where inter-nanotube van der Waals interactions couple the RBMs of bundled carbon nanotubes together. To study the effects of these interactions, we optimized the geometries of homogeneous SWNT and DWNT bundles in vacuum and calculated their RBMs. Each bundle contained seven identical carbon nanotubes, leading to 7 RBMs for SWNTs and 14 RBMs for DWNTs. Two representative geometries are shown in Figure 4.

Data from bundled SWNTs are shown in Figure 5. For nanotubes smaller than 16.5 Å, each RBM is consistent with eq 1 with an added constant b between 0 and 10 cm^{-1}. For nanotubes bigger than 16.5 Å, there is a slight deviation from eq 1 due to distortion of the nanotube sidewall from a radial to a hexagonal shape. See Figure 4a.

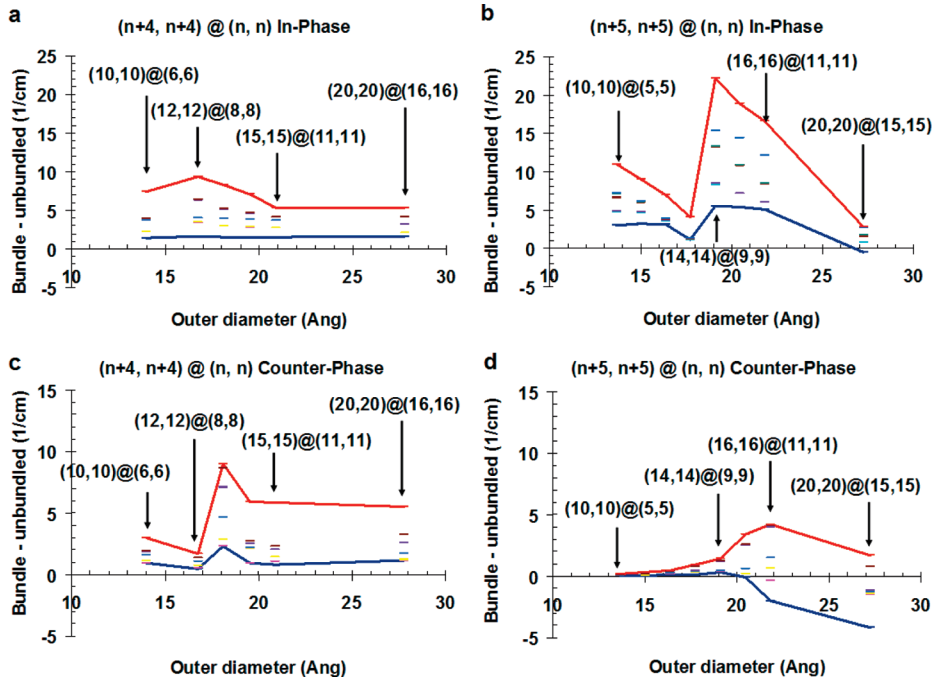

Figure 6. Differences between bundled and unbundled DWNT in-phase and counter-phase radial breathing modes are plotted. Select points are labeled with the outer and inner chiralities of the DWNT. For $(n + 5, n + 5)@(n, n)$ nanotubes, the intershell spacing was around 3.4 Å. The largest deviation from dispersed values of in-phase RMBs was 16.55%, while the largest deviation for counter-phase RBM was −3.02%. For $(n + 4, n + 4)@(n, n)$ nanotubes, the intershell separation was around 3.0−3.1 Å. The largest in-phase deviation was 5.66%, while the largest counter-phase deviation was 3.29%.

For DWNT bundles, two series of geometries were considered. Both series have (n, n) armchair inner shells with either $(n + 5, n + 5)$ or $(n + 4, n + 4)$ outer shells. In each series, the sizes of the inner and outer shells were increased in single increments of chirality and their RBMs calculated. The resulting RBM shifts follow a complicated trend due to the progressive deformation of outer shells into increasingly hexagonal geometries as nanotube size is increased. See Figure 6 for the shift of RBMs in bundled versus unbundled DWNTs.

The counter-phase RBMs of DWNT bundles shifted less than 3.5% compared to corresponding unbundled nanotubes. For in-phase RBMs, the $(n + 4, n + 4)@(n, n)$ DWNT bundles, whose nanotubes have 3.0−3.1 Å intershell separation, experienced 3−6% increases, while the $(n + 5, n + 5)@(n, n)$ DWNT bundles, whose nanotubes had intershell separations of around 3.4 Å, had shifts from 5% to 16.55%. In the $(n + 5, n + 5)@(n, n)$ bundles, there was a rapid increase of the RBM shift from 5% to over 15% when the outer diameter was increased from 17 to 19 Å and a rapid fall back to below 5% with further increases in diameter.

The range of carbon nanotubes sizes and separations tested here are reasonable geometric parameters for real-world DWNTs. Experimenters interpreting RBM data on nanotubes of these approximate sizes need to be mindful of these large frequency shifts if their sample nanotubes are bundled.

Our results give an analytical expression that allows the numerical solution of the inverse problem, namely, finding d_i and d_o for a given pair of in-phase and counter-phase RBMs. An examination of the diameter and separation contour maps for the counter-phase RBM ω_+ and the in-phase RBM ω_- reveals a simple optimization landscape conducive to numerical methods such as simplex optimization. The examination also shows, however, that there are two pairs of inner- and outer-shell diameters for each pair of radial breathing modes. Further complications arise because it is unknown whether both in-phase and counter-phase RBMs will show up at the same excitation energy. Finally, there is the effect of internanotube coupling inside nanotube bundles.

As a test, we applied our method to analyze RBMs reported by Liu, Yu, and Zhang for small diameter DWNTs grown on MgO-supported Fe−Co catalyst.[8] The authors conducted HR-TEM studies showing interlayer separation ranging from 0.35 to 0.42 nm. We believe that two factors complicate interpretation of their HRTEM data. First, HRTEM could sample only a very small portion of the nanotubes produced. Second, the exact thickness of each shell and therefore the separation of shells seen in their HRTEM picture is not unambiguous in light of possible associated amorphous carbon contaminants, defects, and nontrivial scattering of the electron beam. For a broader look at their sample, the authors reported RBM data at 488 nm excitation. The data showed peaks at 150, 158, 197, 227, 257, and 385 cm^{-1}. On the basis of the assumption of independently vibrating shells, the authors interpreted this data as showing that the nanotubes they grew had a narrow d_i distribution from 0.6 to 1.2 nm and a narrow d_o distribution from 1.3 to 2.0 nm.

Table 1 shows an analysis of Liu et al.'s data. Because it is not known which peaks correspond to in-phase modes and which ones to counter-phase modes, we began by taking the highest frequency mode and matching it one by one with lower frequency modes. Then we moved to the next highest frequency mode, and so forth, until all modes were accounted for. We assumed that that intershell separation should be greater than 2.5 Å but less than 6.0 Å and used multiple Nelder−Mead numerical optimization runs to obtain the two converged solutions for each wavenumber pairing. The best solutions are shown in italic.

Simulation results (Figure 6) show that, in DWNT bundles, internanotube coupling shifts the observed RBM wavenumbers. Is this significant for the determination of inner and outer diameters? Assuming the observed RBM is the average value

of the coupling induced peaks, we recalculated diameters after shifting the observed wave numbers by amounts consistent with the simulation. If the 385 cm^{-1} peak remains constant and the 197 cm^{-1} peak is shifted to 191 cm^{-1}, one could get a DWNT with a 13 Å outer diameter and 3.34 Å intershell separation. Similarly, shifting the 257 cm^{-1} peak to 254.5 cm^{-1} and the 158 cm^{-1} peak to 154 cm^{-1} would give two solutions: a 16.6 Å DWNT with 3.34 Å intershell separation and a 17.8 Å nanotube with 3.12 Å intershell separation. In each case, the RBM shifts due to internanotube coupling changed the calculated intershell separation by 0.1 Å, which could affect expected intershell electronic coupling.

Whether or not internanotube coupling is taken into account, our analysis of the Liu, Yu, and Zhang data suggests that their sample contained significant number of DWNTs with intershell separation between 3.1 and 3.4 Å and outer diameters from 13 to 18 Å. This is consistent with their HRTEM pictures considering the ambiguities discussed earlier. Interestingly, the small interlayer separation in these nanotubes could result in a greater proportion of metallic nanotubes due to interlayer electronic structure coupling.[5]

In this paper we calculated the RBMs of a variety of DWNTs. The results of our atomistic simulations show that interlayer and internanotube dispersive coupling significantly affect observed RBMs. We also demonstrate that RBM of DWNTs do not depend explicitly on the chiralities of the inner and outer shells. Instead, an analytical model treating the two shells as homogeneous elastic cylinders coupled by a van der Waals force is sufficient to account for the observed RBM data. Our analytical model gives accurate predictions of RBMs for isolated DWNTs in an experimentally relevant parameter space, and we can use it to predict RBMs for nanotubes given inner and outer diameters or extract possible inner and outer diameters given pairs of in-phase and counter-phase RBMs. Finally, we show that the effects of internanotube coupling in DWNT bundles could affect the calculated intershell separation. As these effects are more difficult to address analytically, a more accurate assessment of the nanotube diameters and separations may require dispersal of the nanotubes using agents such as single-stranded DNA[14] and sodium dodecyl sulfate. We expect that collection of RBM data on individual DWNTs could thus give identifying structural data that could allow correlation between the electronic structure and the geometric structure of DWNTs.

Acknowledgment. We thank Intel Components Research for support in initiating this project and support from the Focus Center Research Program (FCRP) − Center on Functional Engineered Nano Architectonics (FENA) and from NSF (ECS-0609128 and CTS-0608889) in completing it.

Supporting Information Available: Mathematica 7.0 notebook source code for the calculation of RBMs from diameters and of diameters from RBMs is provided under the GPL license; supplemental tables are also provided. This material is available free of charge via the Internet at http://pubs.acs.org.

References and Notes

(1) Lyu, S. C.; Liu, B. C.; Lee, C. J. *Chem. Mater.* **2003**, *15*, 3951–3954.

(2) Hutchingson, J. L.; Kiselev, N. A.; Krinichnaya, E. P.; Krestinin, A. V.; Loutfy, R. O.; Morawsky, A. P.; Muradyan, V. E.; Obraztsova, E. D.; Sloan, J.; Terekhov, S. V.; Zakharov, D. N. *Carbon* **2001**, *39*, 761.

(3) Bandow, S.; Chen, G.; Sumanasekera, G. U.; Gupta, R.; Yudasaka, M.; Iijima, S.; Eklund, P. C. *Phys. Rev. B* **2002**, *66*, 075416.

(4) Kurachi H. et al, *Proceedings of 21st International Display Research Conference/8th International Display Workshops; Society for Information Display*: San Jose, CA, 2001, 1245−1248.

(5) Deng, W.; Goddard, W. A. III;in preparation.

(6) Guo, Y.; Karasawa, N.; Gooddard, W. A. III *Nature (London)* **1991**, *351*, 464.

(7) Wu, G.; Zhou, J.; Dong, J. *Phys. Rev. B* **2005**, *72*, 115418.

(8) Liu, B. C.; Yu, B.; Zhang, M. X. *Chem. Phys. Lett.* **2005**, *407*, 232.

(9) Simon, F.; Kukovecz, A.; Kenya, Z.; Pfeiffer, R.; Kuzmany, H. *Chem. Phys. Lett.* **2005**, *413*, 506–511.

(10) Rahmani, A.; Sauvajol, J.-L.; Cambedouzou, J.; Benoit, C. *Phys. Rev. B* **2005**, *71*, 125402.

(11) Bachilo, S. M.; Strano, M. S.; Kittrell, C.; Hauge, R. H.; Smalley, R. E.; Weisman, R. B. *Science* **2002**, *298*, 2361.

(12) Jorio, A.; Saito, R.; Hafner, J. H.; Lieber, C. M.; Hunter, M.; McClure, T.; Dresselhaus, G.; Dresselhaus, M. S. *Phys. Rev. Lett.* **2001**, *86*, 1118–1121.

(13) Deshpande, V. V.; Chiu, H.-Y.; Postma, H. W. Ch.; Miko, C.; Forro, L.; Bockrath, M. *Nano Letters,* **2006**, *6*, 1092.

(14) Zheng, M.; Jagota, A.; Semke, E. D.; Diner, B. A.; McLean, R. S.; Lustig, S. R.; Richardson, R. E.; Tassi, N. G. *Nat. Mater.* **2003**, *2*, 338.

(15) Hashimoto, A.; Suenaga, K.; Urita, K.; Shimada, T.; Sugai, T.; Bandow, S.; Shinohara, H.; Iijima, S. *Phys. Rev. Lett.* **2005**, *94*, 045504.

JP805828G